

# Universal Anyon Tunneling in a Chiral Luttinger Liquid

Ramon Guerrero-Suarez<sup>1</sup>, Adithya Suresh<sup>1</sup>, Tanmay Maiti<sup>1</sup>, Shuang Liang<sup>1</sup>,  
James Nakamura<sup>1</sup>, Geoffrey Gardner<sup>4</sup>, Claudio Chamon<sup>5</sup>, Michael Manfra<sup>1,2,3,4,\*</sup>

<sup>1</sup>Department of Physics and Astronomy, Purdue University, West Lafayette, 47907, IN, USA.

<sup>2</sup>Elmore Family School of Electrical and Computer Engineering, Purdue University, West Lafayette, 47907, IN, USA.

<sup>3</sup>School of Materials Engineering, Purdue University, West Lafayette, 47907, IN, USA.

<sup>4</sup>Microsoft Quantum Lab West Lafayette, West Lafayette, 47907, IN, USA.

<sup>5</sup>Department of Physics, Boston University, Boston, 02215, MA, USA.

\*Corresponding author Email: [mmanfra@purdue.edu](mailto:mmanfra@purdue.edu).

## Abstract

The edge modes of fractional quantum Hall liquids are described by chiral Luttinger liquid theory. Despite many years of experimental investigation fractional quantum Hall edge modes remain enigmatic with significant discrepancies between experimental observations and detailed predictions of chiral Luttinger liquid theory. Here we report measurements of tunneling conductance between counterpropagating edge modes at  $\nu = 1/3$  across a quantum point contact fabricated on an AlGaAs/GaAs heterostructure designed to promote a sharp confinement potential. We present evidence for tunneling of *anyons* through an  $\nu = 1/3$  incompressible liquid that exhibits universal scaling behavior with respect to temperature, source-drain bias, and barrier transmission, as originally proposed by Wen [1, 2]. We measure the tunneling exponent  $g = 0.334 \pm 0.001$ , consistent with the scaling dimension  $\Delta = g/2 = 1/6$  for a Laughlin quasiparticle at the edge. When combined with measurements of the fractional charge  $e^* = e/3$  and the recently observed anyonic statistical angle  $\theta_a = \frac{2\pi}{3}$ , the measured tunneling exponent fully characterizes the topological order of the primary Laughlin state at  $\nu = 1/3$ .

## Introduction

Three quantities - fractional charge  $e^*$  [3], anyonic statistical angle  $\theta_a$  [4, 5], and the tunneling exponent  $g$  [1, 2], provide a universal parameterization of the topological order [6] of Abelian fractional quantum Hall effect (FQHE) liquids in the Laughlin sequence. The tunneling exponent  $g$  is connected to the scaling dimension,  $\Delta = g/2$ , of the quasiparticles that propagate at the boundary of an incompressible FQHE liquid [1, 2, 6–14]. For Laughlin states,  $g = \nu^{-1}$  for electrons and  $g = \nu$  for fractional quasiparticles, where  $\nu$  is the filling factor of the incompressible state. Although theoretical predictions for these fundamental quantities have been available for more than three decades, experimental validation has proceeded more slowly. Fractionalization of charge was first observed in 1997 following advances in quantum shot noise measurements [15, 16]. Anyonic braiding statistics were demonstrated in 2020 using electronic Fabry-Pérot

interferometers [17–19], and with noise correlation measurements in novel anyon collider experiments [20–22]. Despite these advances, experimental observation of tunneling of anyons and the expected scaling behavior of the chiral Luttinger liquid predicted to exist at the boundary of FQHE liquids have proven to be more elusive. It is theoretically well-established that the properties of the edge modes are a sensitive probe of the bulk topological order, thus reconciling experimental observations with theory remains of paramount importance for full understanding and categorization of FQHE liquid phases.

Counterpropagating edge modes of a fractional quantum Hall liquid may be brought into close proximity to induce tunneling with a quantum point contact (QPC). Early experiments with QPCs in the fractional quantum Hall regime explored behavior with the constriction set to very low transmission [23], the so-called strong backscattering regime. In the strong backscattering limit, the tunneling between the edge modes is mediated by *electrons*. In experiments utilizing elegant cleaved edge

overgrowth heterostructures, Chang and Grayson [24–26] explored tunneling of electrons to the edge of a fractional quantum Hall state from a 3D Fermi gas separated from the edge of a fractional quantum Hall liquid by an AlGaAs tunnel barrier. Although these and other early resonant tunneling experiments [27, 28] gave indications of the impact of strong correlation effects and deviations from the known properties of Fermi liquids, they also revealed important discrepancies with the predictions of chiral Luttinger liquid theory, most notably in the filling factor dependence of the tunneling exponent.

In the weak backscattering limit, when a QPC sufficiently narrows the distance between counterpropagating edge modes that bound an incompressible quantum liquid, weak tunneling between counterpropagating edge modes is expected to be mediated by fractionalized (anyonic) quasiparticles. Previous experiments in the weak tunneling regime at  $\nu = 1/3$  have also shown qualitative and quantitative disagreement with the behavior expected from chiral Luttinger liquid theory [29–33]. Perhaps the most indicative signature of the qualitative inconsistency between experiment and theory was the persistent observation of a *minimum* in tunneling conductance at low bias and lowest temperatures, while theory predicts a *maximum* in zero bias tunneling conductance for a chiral Luttinger liquid at  $\nu = 1/3$ . Qualitative and quantitative differences between experiments and theory remain a fundamental challenge to our understanding of the strongly interacting one-dimensional liquid that forms the boundary of FQHE states. It is important to establish the bulk-boundary correspondence in Abelian Laughlin states if edge-mode dynamics is to be used to probe more exotic non-Abelian topological order [34, 35].

Recent experimental developments give reason for optimism. Veillon *et al.* [36] reported on the determination of the scaling dimension of Abelian FQHE liquids by examination of the crossover from thermal noise to shot noise following a recent theoretical analysis [37, 38]. Germane to the work discussed here, an impressive scaling behavior of conductance was recently demonstrated in a graphene device operating in the quantum Hall regime [39]. This innovative experiment measured the tunneling of *electrons* into a  $\nu = 1/3$  edge mode from a counterpropagating  $\nu = 1$  edge mode. Gates were used to tune the local electron density so that the regions of  $\nu = 1$  and  $\nu = 1/3$  were brought in close proximity to allow electron tunneling.

In this work, we present evidence of direct tunneling of *anyons* across a droplet of  $\nu = 1/3$  liquid and demonstrate universal scaling behavior consistent with the theoretical description of a chiral Luttinger liquid. We focus on the weak backscattering regime, where quantitative comparisons with theory are readily made, and we extract  $g = 0.334 \pm 0.001$ , for the tunneling exponent for the  $\nu = 1/3$  state. Furthermore, we demonstrate scaling behavior of the tunneling conductance with respect to temperature,

source-drain bias, and barrier transmission as originally outlined by Wen and collaborators [1, 2, 13, 40].

Our starting point for data analysis is the universal functional form of the tunneling current originally derived by Wen [2]. This formulation was derived using perturbation theory assuming a small tunnel coupling between counterpropagating edge modes, and yields the tunneling differential conductance

$$G_t = \frac{e^2}{h} \left( \frac{2\pi T}{T_0} \right)^{2g-2} f_g \left( e^* \frac{V_{SD}}{k_B T} \right) \quad (1)$$

where  $T$  is the electron temperature,  $T_0$  is an effective temperature scale proportional to the tunnel coupling between the edge modes, and  $V_{SD}$  is the applied source-drain bias.  $e^*$  is the fractional charge of the quasiparticle that undergoes tunneling and  $g$  is the tunneling exponent. The scaling function  $f_g(x)$  is:

$$f_g(x) = B \left( g + i \frac{x}{2\pi}, g - i \frac{x}{2\pi} \right) \cosh(x/2) \times \left\{ \pi - 2 \tanh(x/2) \operatorname{Im} \left[ \psi \left( g + i \frac{x}{2\pi} \right) \right] \right\} \quad (2)$$

where  $B(a, b)$  is the beta function and  $\psi(x)$  is the digamma function. This universal scaling form, along with the constraints from the chiral Luttinger liquid theory that  $e^* = \nu e$  and  $g = \nu$  for quasiparticle tunneling, produces strict predictions for measurements of the tunneling conductance.

## Device Configuration and Measurement Results

The device studied in this experiment utilizes a quantum point contact which is a functional component of a Fabry-Pérot interferometer [41]. This interferometer was previously used to demonstrate anyonic braiding statistics in the fractional quantum Hall effect at filling factor  $\nu = 2/5$  [19]. It has two QPCs and a pair of plunger gates that define the interference path when in operation. The arms of the QPC are separated by 300 nm and the plunger gates are 1  $\mu\text{m}$  apart. A false color scanning electron microscopy image of a nearly identical device with a schematic of the measurement circuit is shown in Fig. 1a. Only the highlighted QPC is energized to study tunneling phenomena, while all other gates are held at ground potential, including the large gate positioned above the interior of the interferometer. Importantly, this device was fabricated on a GaAs/AlGaAs heterostructure that we identify as the screening well design [17–19, 42, 43]. Two additional quantum wells placed above and below the principal quantum well are populated with high-density two-dimensional electron gases. These screening wells, situated 25 nm above and below the principal quantum well, create a sharp confinement potential at the location of the QPC in the central well; sharp confinement

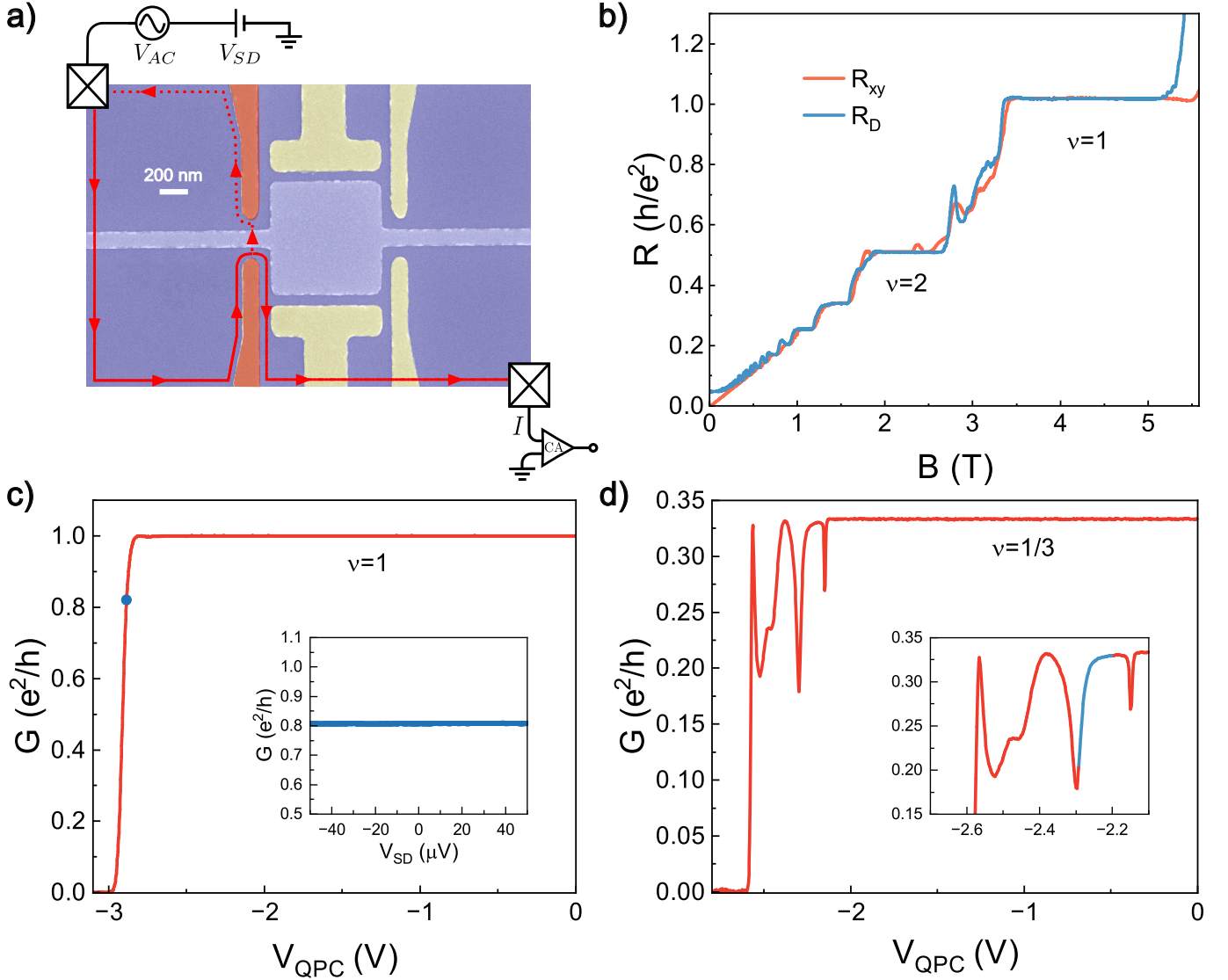


**Fig. 1** (a) False color scanning electron microscopy image of a full interferometer with a schematic of the measurement circuit used in this experiment. The QPC used for tunneling measurements is highlighted in orange. All other gates are grounded. Red lines represent edge mode circulation. (b) Simultaneous measurement of bulk  $R_{xy}$  and  $R_D$  across the QPC as a function of magnetic field at  $T_{mc} = 10$  mK. The QPC is biased just past depletion to define the current path. The filling factor is the same in the QPC as in the bulk of the Hall bar. (c) QPC conductance at the center of the  $\nu = 1$  ( $B = 4.20$  T) plateau. The conductance is quantized to  $e^2/h$  over most of the voltage range and exhibits a sharp pinch-off. This data indicates a sharp confining potential in our QPC built upon the screening well heterostructure design. The inset displays differential conductance at  $\nu = 1$ . This constant differential conductance is expected for the  $\nu = 1$  edge described by Fermi liquid theory, in sharp contrast to the behavior observed at  $\nu = 1/3$ . (d) QPC conductance at  $\nu = 1/3$ . The conductance is quantized to  $e^2/3h$  over most of the voltage range and displays a sharp pinch-off. Unlike the behavior observed at  $\nu = 1$ , a few sharp resonances are observed at  $\nu = 1/3$  prior to full depletion. The inset highlights the region where tunneling was investigated.

produces high edge mode velocity and is critical to the prevention of edge reconstruction [40] that may confound interpretation of tunneling data. This characteristic may account for the differences between the results presented here and previous experimental investigations of tunneling using QPCs in the fractional quantum Hall regime in AlGaAs/GaAs heterostructures [27, 29–31, 33, 36, 44, 45]. To avoid parallel conduction through the screening wells, we utilize depletion gates above and below the arms connecting the ohmic contacts to the interferometer [46]. These gates are negatively biased to locally deplete the

top and bottom screening wells in a small region around the contacts, but leave the main quantum well fully populated and connected to the ohmic leads (see Supplementary Information and Fig. S1b for more details). The electron density of the main quantum well is  $n \approx 1.0 \times 10^{11} \text{cm}^{-2}$  and its mobility is  $\mu \approx 9 \times 10^6 \text{cm}^2/\text{Vs}$  in the fully fabricated device geometry. All conductance measurements are made with standard lock-in techniques with an AC excitation bias of  $2 \mu\text{V}$  and an excitation frequency of 11 Hz. We measure the AC current transmitted through the QPC while varying device parameters

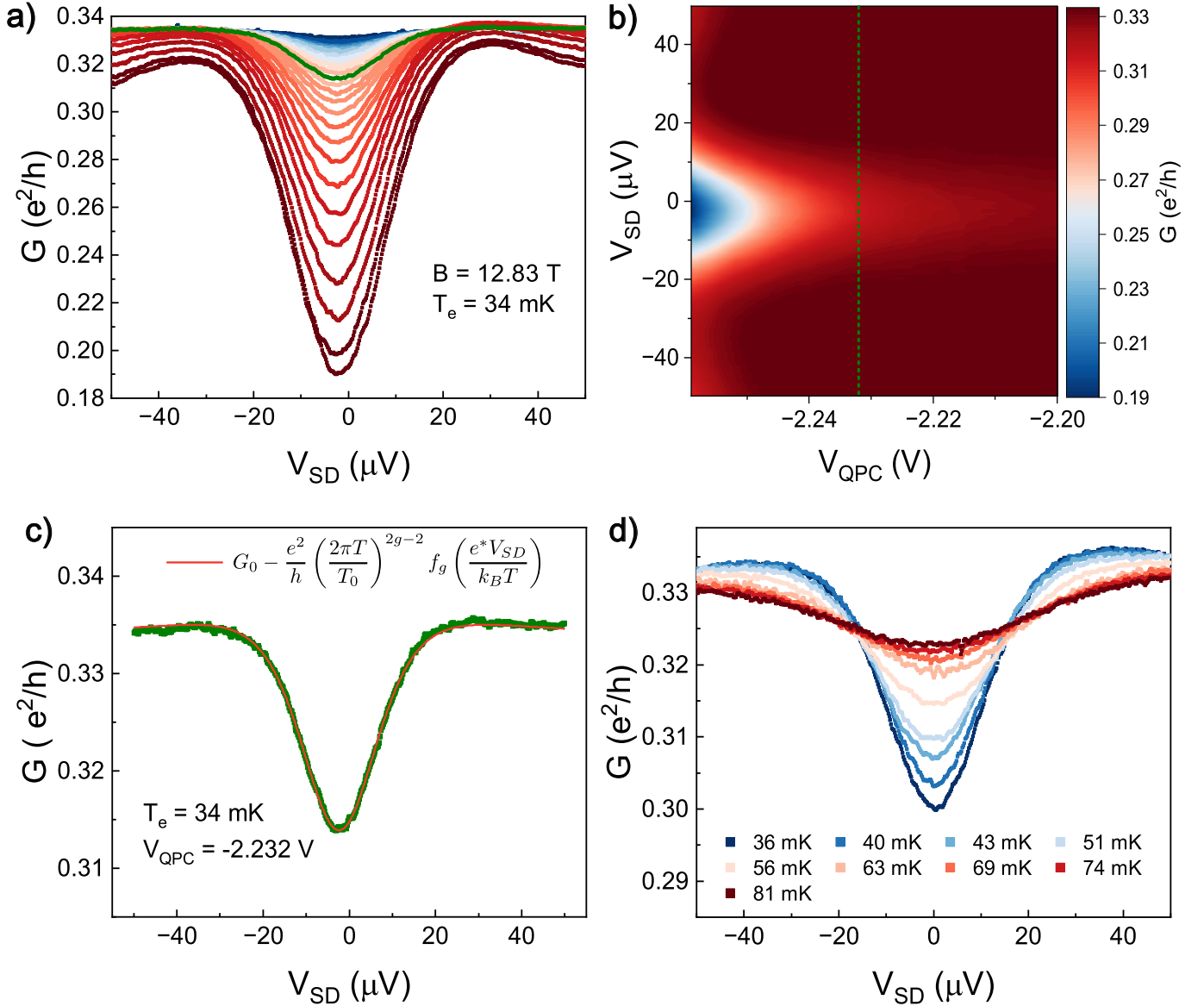


**Fig. 2** (a) Differential conductance measured at several QPC transmissions (see inset Fig. 1a) at fixed electron temperature  $T_e=34$  mK at the center of the  $\nu = 1/3$  plateau. The transmission through the QPC varies from  $t \approx 0.99$  to  $t \approx 0.65$ . (b) 2D color map of differential conductance plotted as a function of QPC voltage and DC source-drain bias  $V_{SD}$ . Fig. 2a are individual linecuts extracted from the data of Fig. 2b. (c) Differential conductance at  $t = 0.94$ . The red line shows the fit to the data using the scaling function introduced by Wen and collaborators [1, 2, 13, 40]. (d) Temperature dependence of the differential conductance for QPC transmission  $t = 0.9$ . Temperatures listed in the legend are mixing chamber temperatures at which each data set was collected.

including DC source-drain bias  $V_{SD}$ , QPC transmission  $t$ , electron temperature  $T_e$ , and applied magnetic field  $B$ . The differential conductance  $G = \frac{\partial I}{\partial V}|_{V_{SD}}$  is the conductance measured at specific values of DC source-drain bias  $V_{SD}$ . The tunneling conductance  $G_t = \frac{\partial I_t}{\partial V}|_{V_{SD}}$  measures the current scattered to the counterpropagating edge across the QPC. In our measurement configuration, the conductance  $G$  is directly measured and the tunneling conductance is given by:  $G_t = G_0 - G$  with  $G_0 = \frac{e^2}{3h}$  at  $\nu = 1/3$  and  $G_0 = \frac{e^2}{h}$  at  $\nu = 1$ . We study tunneling between counterpropagating edges at filling fractions  $\nu = 1$  and  $\nu = 1/3$  in the weak tunneling regime, defined

as  $G_t \ll \sigma_{xy}$  where  $\sigma_{xy}$  is the Hall conductance. In the limit of sharp confining potential, only a single chiral edge mode is observed at  $\nu = 1$  and  $\nu = 1/3$ .

Fig. 1b displays magnetotransport through the device. We simultaneously measure the bulk Hall resistance  $R_{xy}$  measured on the mesa but away from the QPC, and the diagonal resistance  $R_D$  measured through the QPC. This measurement is performed with  $V_{QPC} = -0.4$  V, just past the depletion point of the principal quantum well. As seen in Fig. 1b,  $R_{xy}$  and  $R_D$  coincide at all integer quantum Hall states, indicating that the filling fraction in the QPC is the same as the bulk filling fraction and supports

incompressible states within the QPC. The centers of the  $\nu = 1$  and  $\nu = 1/3$  plateaus are located at  $B = 4.20$  T and  $B = 12.83$  T respectively.

In the weak backscattering regime, tunneling between counterpropagating edge modes is mediated by electrons at  $\nu = 1$  and by fractionalized anyons across a gapped fractional quantum Hall liquid at  $\nu = 1/3$ . Fig. 1c displays the conductance with zero DC source-drain bias as a function of the QPC voltage at the center of the  $\nu = 1$  plateau. We then set the QPC voltage to partially reflect the single  $\nu = 1$  edge mode with transmission  $t \approx 0.8$  and measure the differential conductance as a function of  $V_{SD}$ . The edge mode at  $\nu = 1$  is expected to behave as a normal Fermi liquid of electrons. Ohmic behavior is expected with constant differential conductance, consistent with the data displayed in the inset of Fig. 1c. With confirmation of ohmic behavior at  $\nu = 1$ , we then raise the magnetic field to  $B = 12.83$  T, the center of the  $\nu = 1/3$  plateau. As evident in Fig. 1d, the conductance through the QPC remains quantized over most of the QPC voltage range in a manner similar to that observed at  $\nu = 1$ , but also exhibits a few sharp resonances before full depletion. These resonances are a fingerprint of the specific mesoscopic disorder configuration at  $\nu = 1/3$  in this QPC. The inset to Fig. 1d highlights the region where we measure differential conductance in the weak tunneling regime. The sharp pinch-off observed at both  $\nu = 1$  and  $\nu = 1/3$  indicates that the QPC produces a sharp confinement potential consistent with the screening well heterostructure design and our previous interferometry results [17–19, 42]. If the edge confining potential is not sharp, the edge mode velocity is reduced and edge mode reconstruction is possible [44, 47, 48]. Edge mode reconstruction may be the root cause of the long-standing discrepancy between predictions of chiral Luttinger liquid theory and previous experimental studies of quasiparticle tunneling [29, 30, 33, 44, 45].

The edge at  $\nu = 1/3$  is described as a single chiral charge mode [1, 2, 8]. The tunneling conductance in the weak backscattering limit has been calculated in perturbation theory and is given by (1). For the  $\nu = 1/3$  Laughlin state, it is expected that the scaling exponent  $g$  in equation (1) will be quantized to the universal value  $g = 1/3$ . In the scaling function (1),  $T_0$  is an energy scale that represents the strength of anyon tunneling and is proportional to the QPC transmission determined by the voltage applied to the gates. Fig. 2a displays the differential conductance at a fixed electron temperature  $T_e = 34$  mK while the QPC transmission is varied. We note that  $T_e$  refers to the electron temperature measured concurrently by Coulomb blockade thermometry using the full interferometer as a quantum dot. This approach allows us to accurately measure the electronic temperature in the operating device. The QPC transmission is varied from  $t \approx 0.99$  to  $t \approx 0.65$ . Importantly, the dependence of the conductance on  $V_{SD}$  at  $\nu = 1/3$  displays

the expected functional dependence predicted by chiral Luttinger liquid theory in the weak tunneling limit. At high bias the differential conductance saturates to the quantized value of  $e^2/3h$ . The zero bias ( $V_{SD} = 0$ ) conductance also displays a pronounced minimum. To the best of our knowledge, this qualitative behavior of a minimum in differential conductance at zero DC bias and saturation to  $G = \frac{e^2}{3h}$  has not been observed previously in experiments in which tunneling between fractional quantum Hall edge modes was studied in the weak tunneling limit at  $\nu = 1/3$  [29, 30, 36].

Our data not only reproduces the qualitative behavior predicted by chiral Luttinger liquid theory, but significantly, facilitates extraction of the scaling exponent with high precision. Fig. 2c displays the differential conductance with  $t = 0.94$  at  $T_e = 34$  mK along with a least squares fit to equation (1). In our fit at  $T_e = 34$  mK,  $G_0$ ,  $T_0$  and  $g$  are left as free parameters while  $e^*$  is set to  $e^* = \frac{e}{3}$ . The effective charge of  $\frac{e}{3}$  is independently verified by operating this device as a Fabry-Pérot interferometer at  $\nu = 1/3$  [17–19, 42]. The value extracted for the scaling exponent is  $g = 0.334 \pm 0.001$  with  $T_0 = 1.3$  mK and  $G_0 = 0.3335$ .

It can be seen in equation (1) that the tunneling conductance is a universal function of the dimensionless parameters  $T/T_0$  and  $V/k_B T$ . We now examine the degree to which scaling behavior is manifest in our data. We experimentally examine the dependence of the tunneling conductance on  $T/T_0$ , using two approaches. First, we keep the electron temperature fixed and vary the QPC transmission  $t$  to vary the ratio  $T/T_0$ . In the second set of experiments, we keep the QPC transmission fixed ( $T_0$  constant) and vary the temperature.

The results of the first approach are displayed Fig. 3. The data in Fig. 3a were extracted from the 2D color plot of conductance displayed in Fig. 2b.  $G_0$  and  $T_0$  for each point are extracted from fitting the traces to eqn. (1) with  $T_e = 34$  mK, as was done for the data in Fig. 2c. Theoretical scaling functions *assuming*  $g = 0.3, 1/3, 0.4$  are also plotted. We observe that the data agree well with the expected scaling for precisely  $g = 1/3$ . The robustness of this scaling is tested by repeating the measurement at two different electron temperatures,  $T_e = 47$  mK and  $T_e = 69$  mK, and also at different locations on the  $\nu = 1/3$  plateau ( $\Delta B = \pm 90$  mT away from the center of the plateau). As seen in Figs. 3b and 3c, the data continue to show good agreement with the theoretical prediction  $g = 1/3$ . For this analysis, an accurate electron temperature in the device is extracted using Coulomb blockade (CB) thermometry (see Supplementary Information for more details).

To demonstrate universal scaling in  $V/k_B T$ , we fixed the QPC voltage and measured the differential conductance at several different temperatures. This data is shown in Fig. 2d for QPC transmission of  $t = 0.9$  and dilution refrigerator temperature ranging from  $T = 36$  mK to



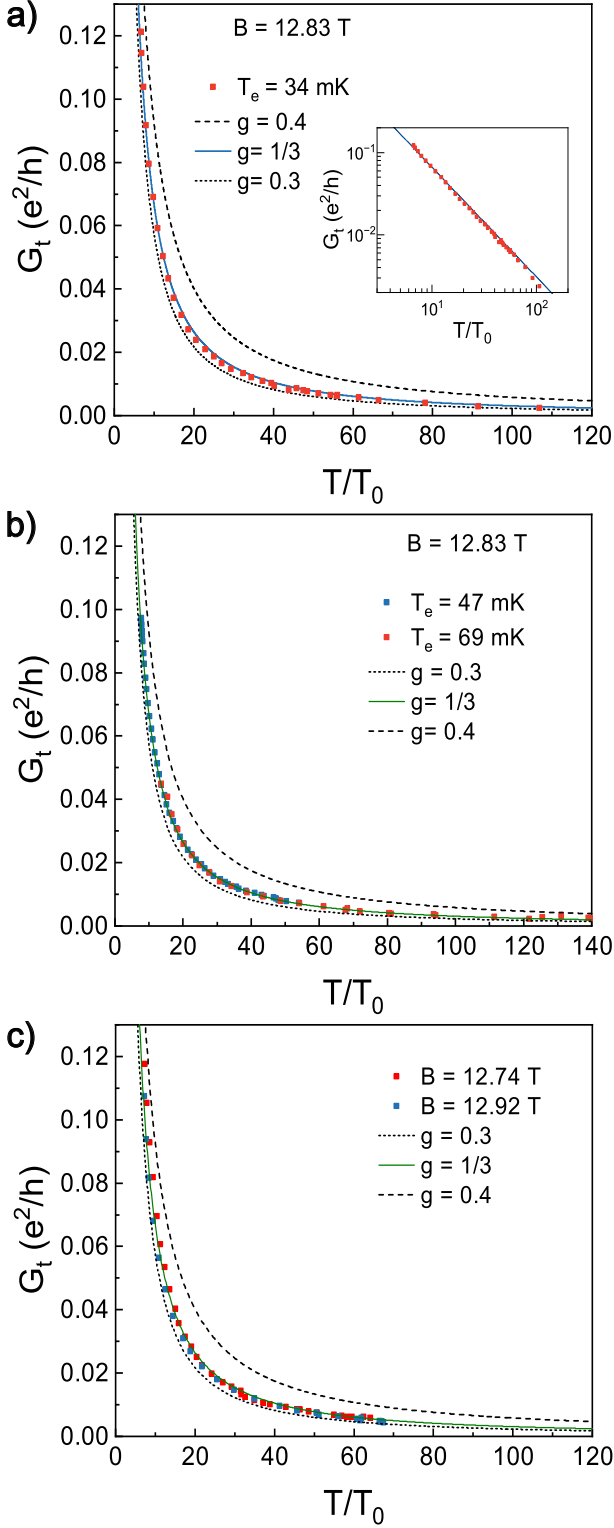


**Fig. 3** (a) Scaling of zero bias tunneling conductance at  $T_e = 34$  mK and  $B = 12.83$  T, at the center of the  $\nu = 1/3$  plateau. The lines correspond to the theoretical expectation at  $g = 1/3$ ,  $g = 0.3$  and  $g = 0.4$ . The inset shows the data plotted on a log-log scale. (b) Scaling of zero bias tunneling conductance at  $T_e = 47$  mK and  $T_e = 69$  mK, at the center of  $\nu = 1/3$ . (c) Scaling of zero bias tunneling conductance at  $B = 12.92$  T and  $B = 12.74$  T, which are  $\Delta B \pm 90$  mT away from the center of the  $\nu = 1/3$  plateau.

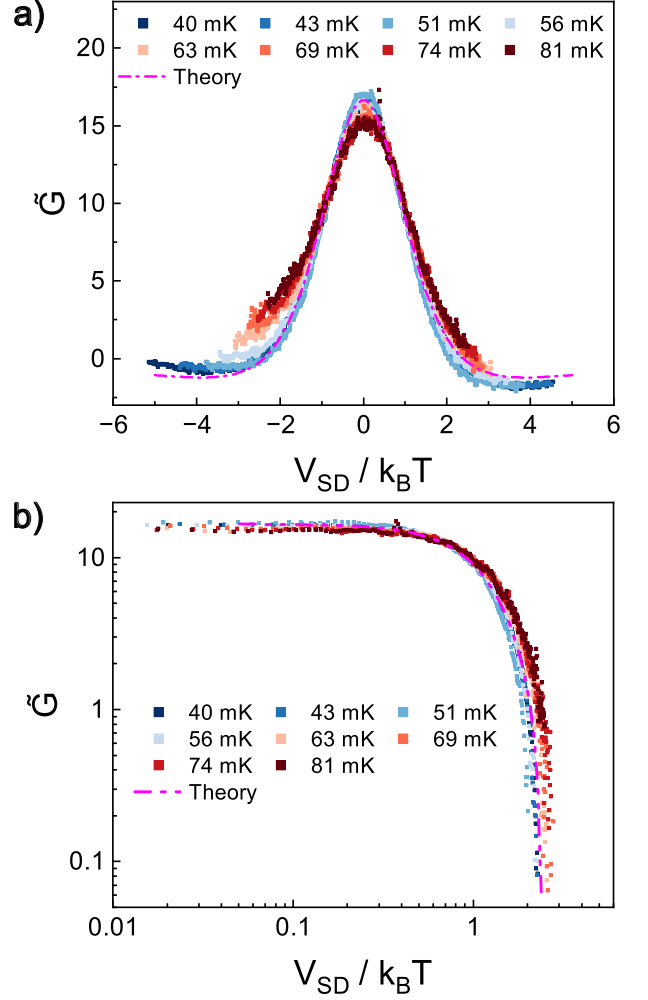


**Fig. 4** (a) Scaling behavior of reduced tunneling conductance  $\tilde{G}$  vs.  $V_{SD}/k_B T$  using data of Fig. 2d. Data collected at different temperatures collapse onto a single curve. Dashed magenta line is the theoretical expectation for  $g = 1/3$ . (b) Data in (a) plotted on log-log scale. Dashed magenta line is the theoretical expectation for  $g = 1/3$ .

$T = 81$  mK. For this data set, we report the mixing chamber temperature, as we do not perform CB thermometry at each temperature setting. To test for scaling behavior, we define  $\tilde{G}$ :

$$\tilde{G} = \frac{h}{e^2} \left( \frac{T_0}{2\pi T} \right)^{2g-2} (G_0 - G) \quad (3)$$

where the tunneling conductance,  $G_0 - G$ , is scaled by an universal coefficient. After rendering the conductance data in Fig. 2d in this manner and plotting  $\tilde{G}$  as a function of  $V/k_B T$ , we observe the scaling collapse displayed in Fig. 4a and b. In Fig. 4a,  $\tilde{G}$  is plotted on a linear scale versus  $V_{SD}/k_B T$ . The reduced conductance at different temperatures collapses into a single curve given by the universal function:

$$\tilde{G} = f_g \left( e^* \frac{V_{SD}}{k_B T} \right) \quad (4)$$

The scaling collapse becomes more evident when  $\tilde{G}$  versus  $V_{SD}/k_B T$  is plotted on a log-log scale as displayed in Fig. 4b.

## Discussion

The data plotted in Figs. 4a and 4b demonstrate that the tunneling conductance obeys robust scaling in the dimensionless variable  $V_{SD}/k_B T$ . In particular, the scaling behavior follows the predictions of chiral Luttinger liquid theory for the  $\nu = 1/3$  state in the weak backscattering limit. The theoretical expectation is indicated by the dashed magenta lines in Figs. 4a and 4b that overlap with the experimental data. One may ask why this behavior has not previously been observed in AlGaAs/GaAs heterostructures used in the study of the fractional quantum Hall effect. The most significant difference between the experiments reported here and previous generations of experiments employing AlGaAs/GaAs heterostructures is the introduction of the screening well heterostructure into our device architecture. Ancillary screening wells have been effectively used to control Coulomb charging effects in the operation of Fabry-Pérot interferometers, and have also been shown to provide a sharper confining potential at the edge of the FQHE liquid [42]. We speculate that the close agreement with the theoretical predictions seen here is due to the absence of edge reconstruction that is typically observed with standard heterostructures. In addition, the filling factor in the QPC is well defined and matches that in the bulk, providing a droplet of incompressible liquid supporting anyon excitations. Under these conditions, the correspondence with predictions for a single chiral Luttinger liquid edge mode is most likely manifest.

## Conclusions

Using a QPC built on an AlGaAs/GaAs screening well heterostructure, we measured tunneling conductance between counterpropagating edge modes of the  $\nu = 1/3$  FQHE state in the weak backscattering limit. Our data facilitate the extraction of the tunneling exponent  $g = 0.334 \pm 0.001$ , consistent with expectations for anyon tunneling into a chiral Luttinger liquid. In addition, we observed scaling behavior in the dimensionless variable  $V_{SD}/k_B T$ . These findings indicate that the classification of the topological order responsible for the bulk quantization of FQHE liquids can be fully characterized by a sequence of measurements with a Fabry-Pérot interferometer.

## Acknowledgments

This research is sponsored by the U.S. Department of Energy, Office of Science, Office of Basic Energy Sciences,

under the award numbers DE-SC0020138 and DE-FG02-06ER46316. The content of the information presented here does not necessarily reflect the position or the policy of the US government, and no official endorsement should be inferred.

## References

- [1] X.G. Wen, Chiral Luttinger liquid and the edge excitations in the fractional quantum Hall states, *Phys. Rev. B* **41**, 12838–12844 (1990). <https://doi.org/10.1103/PhysRevB.41.12838>
- [2] X.G. Wen, Edge transport properties of the fractional quantum Hall states and weak-impurity scattering of a one-dimensional charge-density wave, *Phys. Rev. B* **44**, 5708–5719 (1991). <https://doi.org/10.1103/PhysRevB.44.5708>
- [3] R.B. Laughlin, Anomalous quantum Hall effect: An incompressible quantum fluid with fractionally charged excitations, *Phys. Rev. Lett.* **50**, 1395–1398 (1983). <https://doi.org/10.1103/PhysRevLett.50.1395>
- [4] B.I. Halperin, Statistics of Quasiparticles and the Hierarchy of Fractional Quantized Hall States, *Phys. Rev. Lett.* **52**, 1583–1586 (1983). <https://doi.org/10.1103/physrevlett.52.1583>
- [5] D. Arovas, J.R. Schrieffer, F. Wilczek, Fractional statistics and the quantum Hall effect, *Phys. Rev. Lett.* **53**, 722–723 (1984). <https://doi.org/10.1103/PhysRevLett.53.722>
- [6] X.G. Wen, Topological orders and edge excitations in fractional quantum Hall states, *Advances in Physics* **44**, 405–473 (1995). <https://doi.org/10.1080/00018739500101566>
- [7] C.L. Kane, M.P.A. Fisher, Transport in a one-channel Luttinger liquid, *Phys. Rev. Lett.* **68**, 1220–1223 (1992). <https://doi.org/10.1103/PhysRevLett.68.1220>
- [8] C.L. Kane, M.P.A. Fisher, Transmission through barriers and resonant tunneling in an interacting one-dimensional electron gas, *Phys. Rev. B* **46**, 15233–15262 (1992). <https://doi.org/10.1103/PhysRevB.46.15233>
- [9] C.L. Kane, M.P.A. Fisher, Nonequilibrium noise and fractional charge in the quantum Hall effect, *Phys. Rev. Lett.* **72**, 724–727 (1994). <https://doi.org/10.1103/PhysRevLett.72.724>
- [10] P. Fendley, H. Saleur, N. Warner, Exact solution of a massless scalar field with a relevant boundary

- interaction, Nuclear Physics B **430**, 577–596 (1994). [https://doi.org/10.1016/0550-3213\(94\)90160-0](https://doi.org/10.1016/0550-3213(94)90160-0)
- [11] P. Fendley, A.W.W. Ludwig, H. Saleur, Exact conductance through point contacts in the  $\nu = 1/3$  fractional quantum Hall effect, Phys. Rev. Lett. **74**, 3005–3008 (1995). <https://doi.org/10.1103/PhysRevLett.74.3005>
- [12] P. Fendley, A.W.W. Ludwig, H. Saleur, Exact nonequilibrium transport through point contacts in quantum wires and fractional quantum Hall devices, Phys. Rev. B **52**, 8934–8950 (1995). <https://doi.org/10.1103/PhysRevB.52.8934>
- [13] C. de C. Chamon, X.G. Wen, Resonant tunneling in the fractional quantum Hall regime, Phys. Rev. Lett. **70**, 2605–2608 (1993). <https://doi.org/10.1103/PhysRevLett.70.2605>
- [14] C. de C. Chamon, D.E. Freed, X.G. Wen, Tunneling and quantum noise in one-dimensional Luttinger liquids, Phys. Rev. B **51**, 2363–2379 (1995). <https://doi.org/10.1103/PhysRevB.51.2363>
- [15] R. de Picciotto, M. Reznikov, M. Heiblum, V. Umansky, G. Bunin, D. Mahalu, Direct observation of a fractional charge, Nature **389**, 162–164 (1997). <https://doi.org/10.1038/38241>
- [16] L. Saminadayar, D.C. Glatthli, Y. Jin, B. Etienne, Observation of the  $e/3$  fractionally charged Laughlin quasiparticle, Phys. Rev. Lett. **79**, 2526–2529 (1997). <https://doi.org/10.1103/PhysRevLett.79.2526>
- [17] J. Nakamura, S. Liang, G.C. Gardner, M.J. Manfra, Direct observation of anyonic braiding statistics, Nature Physics **16**, 931–936 (2020). <https://doi.org/10.1038/s41567-020-1019-1>
- [18] J. Nakamura, S. Liang, G.C. Gardner, M.J. Manfra, Impact of bulk-edge coupling on observation of anyonic braiding statistics in quantum Hall interferometers, Nature Communications **13** (2022). <https://doi.org/10.1038/s41467-022-27958-w>
- [19] J. Nakamura, S. Liang, G.C. Gardner, M.J. Manfra, Fabry-Pérot interferometry at the  $\nu = 2/5$  fractional quantum Hall state, Phys. Rev. X **13**, 041012 (2023). <https://doi.org/10.1103/PhysRevX.13.041012>
- [20] H. Bartolomei, M. Kumar, R. Bisognin, A. Marguerite, J.M. Berroir, E. Bocquillon, B. Plaçais, A. Cavanna, Q. Dong, U. Gennser, Y. Jin, G. Fève, Fractional statistics in anyon collisions, Science **368**, 173–177 (2020). <https://doi.org/10.1126/science.aaz5601>
- [21] M. Ruelle, E. Frigerio, J.M. Berroir, B. Plaçais, J. Rech, A. Cavanna, U. Gennser, Y. Jin, G. Fève, Comparing fractional quantum Hall Laughlin and Jain topological orders with the anyon collider, Phys. Rev. X **13**, 011031 (2023). <https://doi.org/10.1103/PhysRevX.13.011031>
- [22] J.Y.M. Lee, C. Hong, T. Alkalay, N. Schiller, V. Umansky, M. Heiblum, Y. Oreg, H.S. Sim, Partitioning of diluted anyons reveals their braiding statistics, Nature **617**, 277–281 (2023). <https://doi.org/10.1038/s41586-023-05883-2>
- [23] F. Milliken, C. Umbach, R. Webb, Indications of a Luttinger liquid in the fractional quantum Hall regime, Solid State Communications **97**, 309–313 (1996). [https://doi.org/10.1016/0038-1098\(95\)00181-6](https://doi.org/10.1016/0038-1098(95)00181-6)
- [24] A.M. Chang, L.N. Pfeiffer, K.W. West, Observation of chiral Luttinger behavior in electron tunneling into fractional quantum Hall edges, Phys. Rev. Lett. **77**, 2538–2541 (1996). <https://doi.org/10.1103/PhysRevLett.77.2538>
- [25] M. Grayson, D.C. Tsui, L.N. Pfeiffer, K.W. West, A.M. Chang, Continuum of chiral Luttinger liquids at the fractional quantum Hall edge, Phys. Rev. Lett. **80**, 1062–1065 (1998). <https://doi.org/10.1103/PhysRevLett.80.1062>
- [26] A.M. Chang, M.K. Wu, C.C. Chi, L.N. Pfeiffer, K.W. West, Plateau behavior in the chiral Luttinger liquid exponent, Phys. Rev. Lett. **86**, 143–146 (2001). <https://doi.org/10.1103/PhysRevLett.86.143>
- [27] V.J. Goldman, B. Su, Resonant tunneling in the quantum Hall regime: Measurement of fractional charge, Science **267**, 1010–1012 (1995). <https://doi.org/10.1126/science.267.5200.1010>
- [28] I. Maasilta, V. Goldman, Line shape of resonant tunneling between fractional quantum Hall edges, Phys. Rev. B **55**, 4081 (1997). <https://doi.org/10.1103/PhysRevB.55.4081>
- [29] S. Roddaro, V. Pellegrini, F. Beltram, G. Biasiol, L. Sorba, R. Raimondi, G. Vignale, Nonlinear quasiparticle tunneling between fractional quantum Hall edges, Phys. Rev. Lett. **90**, 046805 (2003). <https://doi.org/10.1103/PhysRevLett.90.046805>
- [30] S. Roddaro, V. Pellegrini, F. Beltram, G. Biasiol, L. Sorba, Interedge strong-to-weak scattering evolution at a constriction in the fractional quantum Hall regime, Phys. Rev. Lett. **93**, 046801 (2004). <https://doi.org/10.1103/PhysRevLett.93.046801>



- [31] S. Roddaro, V. Pellegrini, F. Beltram, Quasi-particle tunneling at a constriction in a fractional quantum Hall state, *Solid State Communications* **131**, 565–572 (2004). <https://doi.org/10.1016/j.ssc.2004.05.049>
- [32] S. Baer, C. Rössler, T. Ihn, K. Ensslin, C. Reichl, W. Wegscheider, Experimental probe of topological orders and edge excitations in the second Landau level, *Phys. Rev. B* **90**, 075403 (2014). <https://doi.org/10.1103/PhysRevB.90.075403>
- [33] S. Hennel, P. Scheidegger, M. Kellermeier, A. Hofmann, T. Krähenmann, C. Reichl, W. Wegscheider, T. Ihn, K. Ensslin, Quasiparticle tunneling in the lowest Landau level, *Phys. Rev. B* **97**, 245305 (2018). <https://doi.org/10.1103/PhysRevB.97.245305>
- [34] J.B. Miller, I.P. Radu, D.M. Zumbühl, E.M. Levenson-Falk, M.A. Kastner, C.M. Marcus, L.N. Pfeiffer, K.W. West, Fractional quantum Hall effect in a quantum point contact at filling fraction  $5/2$ , *Nature Physics* **3**, 561–565 (2007). <https://doi.org/10.1038/nphys658>
- [35] I.P. Radu, J.B. Miller, C.M. Marcus, M.A. Kastner, L.N. Pfeiffer, K.W. West, Quasi-particle properties from tunneling in the  $\nu = 5/2$  fractional quantum Hall state, *Science* **320**, 899–902 (2008). <https://doi.org/10.1126/science.1157560>
- [36] A. Veillon, C. Piquard, P. Glidic, Y. Sato, A. Aassime, A. Cavanna, Y. Jin, U. Gennser, A. Anthore, F. Pierre, Observation of the scaling dimension of fractional quantum Hall anyons, *Nature* **632**, 517–521 (2024). <https://doi.org/10.1038/s41586-024-07727-z>
- [37] K. Snizhko, V. Cheianov, Scaling dimension of quantum Hall quasiparticles from tunneling-current noise measurements, *Phys. Rev. B* **91**, 195151 (2015). <https://doi.org/10.1103/PhysRevB.91.195151>
- [38] N. Schiller, Y. Oreg, K. Snizhko, Extracting the scaling dimension of quantum Hall quasiparticles from current correlations, *Phys. Rev. B* **105**, 165150 (2022). <https://doi.org/10.1103/physrevb.105.165150>. [2111.05399](https://arxiv.org/abs/2111.05399)
- [39] L.A. Cohen, N.L. Samuelson, T. Wang, T. Taniguchi, K. Watanabe, M.P. Zaletel, A.F. Young, Universal chiral Luttinger liquid behavior in a graphene fractional quantum Hall point contact, *Science* **382**, 542–547 (2023). <https://doi.org/10.1126/science.adf9728>
- [40] C. de C. Chamon, X.G. Wen, Sharp and smooth boundaries of quantum Hall liquids, *Phys. Rev. B* **49**, 8227–8241 (1994). <https://doi.org/10.1103/PhysRevB.49.8227>
- [41] C. de C. Chamon, D.E. Freed, S.A. Kivelson, S.L. Sondhi, X.G. Wen, Two point-contact interferometer for quantum Hall systems, *Phys. Rev. B* **55**, 2331–2343 (1997). <https://doi.org/10.1103/PhysRevB.55.2331>
- [42] J. Nakamura, S. Fallahi, H. Sahasrabudhe, R. Rahman, S. Liang, G.C. Gardner, M.J. Manfra, Aharonov–Bohm interference of fractional quantum Hall edge modes, *Nature Physics* **15**, 563–569 (2019). <https://doi.org/10.1038/s41567-019-0441-8>
- [43] S. Liang, J. Nakamura, G.C. Gardner, M.J. Manfra, Single electron interference and capacitive edge mode coupling generates  $\phi_0/2$  flux periodicity in Fabry–Pérot interferometers in the integer quantum Hall regime, *arXiv preprint arXiv:2502.00124* (2025)
- [44] R. Bhattacharyya, M. Banerjee, M. Heiblum, D. Mahalu, V. Umansky, Melting of interference in the fractional quantum Hall effect: Appearance of neutral modes, *Phys. Rev. Lett.* **122**, 246801 (2019). <https://doi.org/10.1103/PhysRevLett.122.246801>
- [45] N. Schiller, T. Alkalay, C. Hong, V. Umansky, M. Heiblum, Y. Oreg, K. Snizhko, Scaling tunnelling noise in the fractional quantum Hall effect tells about renormalization and breakdown of chiral Luttinger liquid, *arXiv preprint arXiv:2403.17097* (2024)
- [46] J. Eisenstein, L. Pfeiffer, K. West, Independently contacted two-dimensional electron systems in double quantum wells, *Applied Physics Letters* **57**, 2324–2326 (1990). <https://doi.org/10.1063/1.103882>
- [47] B. Rosenow, B.I. Halperin, Nonuniversal behavior of scattering between fractional quantum Hall edges, *Phys. Rev. Lett.* **88**, 096404 (2002). <https://doi.org/10.1103/PhysRevLett.88.096404>
- [48] E. Papa, A.H. MacDonald, Interactions suppress quasiparticle tunneling at Hall bar constrictions, *Phys. Rev. Lett.* **93**, 126801 (2004). <https://doi.org/10.1103/PhysRevLett.93.126801>

## Supplementary Information

### AlGaAs/GaAs Heterostructure and Device Operation

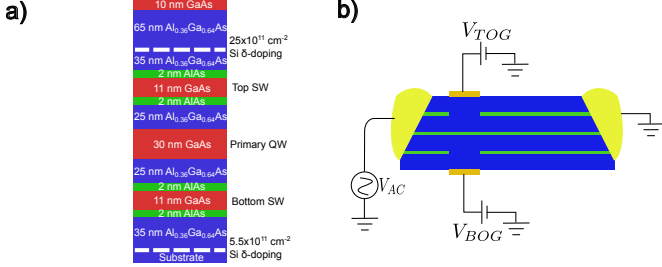


**Fig. S1** (a) GaAs/AlGaAs screening well heterostructure stack. Two 11nm thick GaAs screening wells flank the primary 30nm GaAs quantum well. (b) Schematic of the proximal gates to the ohmic contacts used to limit transport to the primary quantum well. The three quantum wells are in contact with an ohmic contact held at ground potential, but only the primary quantum well is connected to the excitation voltage. The top (bottom) screening well is isolated using a top (bottom) gate set at  $V_{T OG}$  ( $V_{B OG}$ ). This device design allows the screening wells to be held at a fixed potential while transport occurs only through the primary quantum well.

The GaAs/AlGaAs heterostructure used in this study was grown using molecular beam epitaxy. The layer stack is shown in Fig. S1. The primary quantum well has a density of  $n = 1.0 \times 10^{11} \text{ cm}^{-2}$  and mobility of  $\mu = 9 \times 10^6 \text{ cm}^2/\text{Vs}$ . The heterostructure incorporates additional screening wells separated by a 25nm from the primary quantum well. For device operation, we want transport to occur only through the primary quantum well. The screening wells are isolated from the ohmic contacts using top and bottom metallic gates. These gates are located near the ohmic contacts far from the mesoscopic region that defines the Fabry-Pérot interferometer. Negative voltage is applied to deplete the screening wells only in a narrow region around the ohmic contacts (see Fig. S1b).

### Coulomb Blockade Thermometry

As the QPC used for our measurements of tunneling conductance is part of a  $1\mu\text{m}^2$  interferometer, the electronic temperature of the device can be extracted by Coulomb blockade thermometry when the interferometer is operated as a quantum dot connected the two-dimensional electron gas via tunnel barriers. We measured the charging energy of this quantum dot to be  $e^2/C \approx 91\mu\text{eV}$  and the lever arm  $\alpha \approx 0.016$ . The zero bias conductance  $G$  as a function of the plunger voltage  $V_{pg}$  can then be fitted to  $G \propto \cosh^{-2}(\alpha V_{pg}/2k_bT)$  to extract the temperature under various measurement conditions (see Fig. S2). This technique allows for accurate temperature measurements of the electron bath in an operating device.

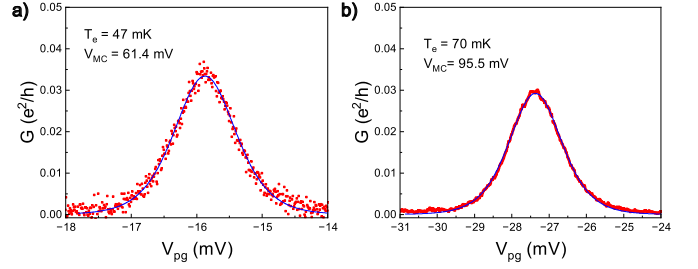


**Fig. S2** (a) Conductance in the Coulomb blockade regime as a function of plunger gate voltage. For this measurement, an excitation voltage  $V_{MC} = 61.4 \text{ mV}$  is applied to the mixing chamber heater, and the system has been allowed to equilibrate. (b) Same as (a) but with  $V_{MC} = 95.5 \text{ mV}$ .

### Additional Data Sets

The data displayed in Fig. 2d of the main text shows the temperature dependence of the differential conductance at a particular QPC transmission,  $t = 0.9$ . We measured the temperature dependence at several additional values of QPC transmission in the weak backscattering limit. This data is displayed in Fig. S3.

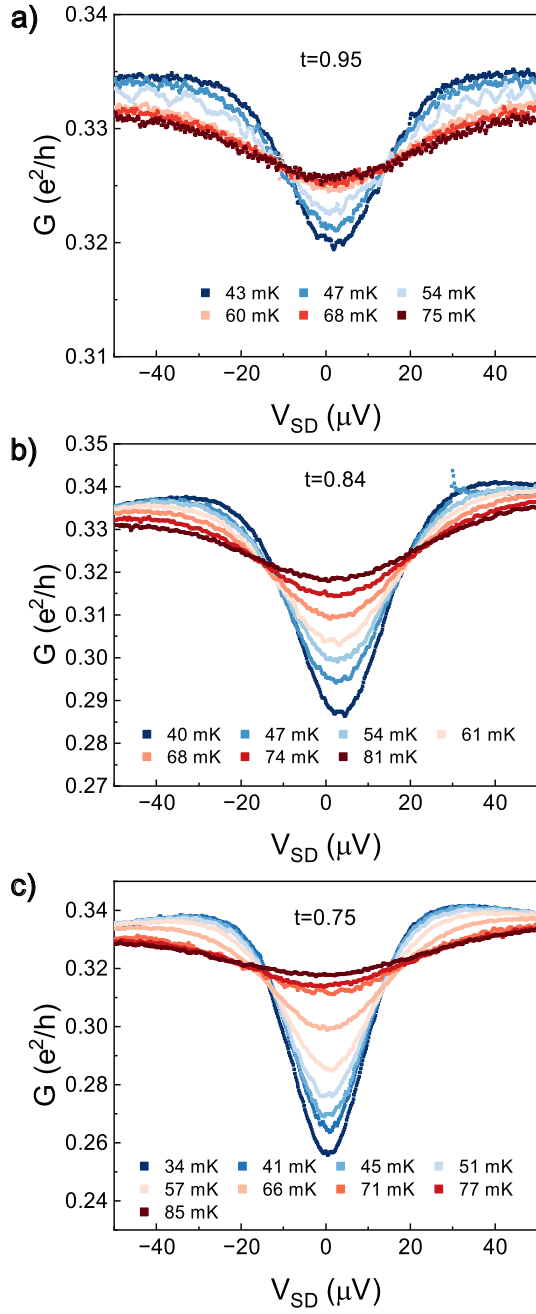


**Fig. S3** (a) Temperature dependence of the differential conductance for QPC transmission  $t = 0.95$ . Temperatures listed in the legend are mixing chamber temperatures at which each data set was collected. (b) Same as (a) but with  $t = 0.84$ . (c) Same as (a) but with  $t = 0.75$ .